AFRL-AFOSR-VA-TR-2016-0158

Magnetic-Field-Assisted Assembly of Ordered Multifunctional Ceramic Nanocomposites for Extreme Environments

Konstantin KORNEV
CLEMSON UNIVERSITY

04/01/2016
Final Report

Air Force Research Laboratory
AF Office Of Scientific Research (AFOSR)/ RTB1
Arlington, Virginia 22203
Air Force Materiel Command

REPORT DOCUMENTATION PAGE

Form Approved
OMB No. 0704-0188

1. REPORT DATE *(DD-MM-YYYY)*	2. REPORT TYPE	3. DATES COVERED *(From - To)*
24-04-2016	Final Performance	15 Sep 2012 to 14 Nov 2017

4. TITLE AND SUBTITLE
Magnetic-Field-Assisted Assembly of Ordered Multifunctional Ceramic Nanocomposites for Extreme Environments

5a. CONTRACT NUMBER

5b. GRANT NUMBER
FA9550-12-1-0459

5c. PROGRAM ELEMENT NUMBER
61102F

6. AUTHOR(S)
Konstantin KORNEV

5d. PROJECT NUMBER

5e. TASK NUMBER

5f. WORK UNIT NUMBER

7. PERFORMING ORGANIZATION NAME(S) AND ADDRESS(ES)
CLEMSON UNIVERSITY
201 SIKES HALL
CLEMSON, SC 29634-0001 US

8. PERFORMING ORGANIZATION REPORT NUMBER

9. SPONSORING/MONITORING AGENCY NAME(S) AND ADDRESS(ES)
AF Office of Scientific Research
875 N. Randolph St. Room 3112
Arlington, VA 22203

10. SPONSOR/MONITOR'S ACRONYM(S)
AFRL/AFOSR RTB1

11. SPONSOR/MONITOR'S REPORT NUMBER(S)
AFRL-AFOSR-VA-TR-2016-0158

12. DISTRIBUTION/AVAILABILITY STATEMENT
A DISTRIBUTION UNLIMITED: PB Public Release

13. SUPPLEMENTARY NOTES

14. ABSTRACT

The goal of this project was to explore physics, materials and surface chemistry behind the polymer-based route towards creation of magnetic
ceramic composites out of magnetic nanorods and nanofibers. We successfully developed the experimental protocol aimed to make mullite coating
films with embedded magnetic inclusions. Electrospun mullite nanofibers with incorporated magnetic nanoparticles, SiC whiskers decorated with
magnetic nanoparticles, and Nickel nanorods were successfully embedded into mullite films. We developed an experimental procedure guarantying
the reproducible preparation of magnetic silicon carbide (mSiC) whiskers for the use as fillers in the mullite based composite films. We studied
kinetics of collective alignment of nanorods and fibers in mullite precursor undergoing a sol/gel transition under uniform magnetic field. These
studies resulted in a successful development of the experimental protocol for controlled alignment of nanorods/nanofibers in thin films prior to the
complete solidification of the film. Crack-free magnetic composite films with mullite matrix have been synthesized and characterized. Fifteen
papers were published based on the results of this project.

15. SUBJECT TERMS
carbon nanotubes, composite, electromagnetic shielding, extreme environments, magnetism, fibers, woven composite, boron nitride, silicon carbide, microwave, nanorods

Standard Form 298 (Rev. 8/98)
Prescribed by ANSI Std. Z39.18

16. SECURITY CLASSIFICATION OF:			17. LIMITATION OF ABSTRACT	18. NUMBER OF PAGES	19a. NAME OF RESPONSIBLE PERSON
a. REPORT	b. ABSTRACT	c. THIS PAGE			SAYIR, ALI
Unclassified	Unclassified	Unclassified	UU		19b. TELEPHONE NUMBER *(Include area code)* 703-696-7236

Standard Form 298 (Rev. 8/98)
Prescribed by ANSI Std. Z39.18

Final Report

Magnetic-field-assisted assembly of ordered multifunctional ceramic nanocomposites for extreme environments, FA9550-12-1-0459

Konstantin G. Kornev (PI), Igor Luzinov, & Fei Peng

Department of Material Science and Engineering, Clemson University

kkornev@clemson.edu

In collaboration with

Jeffery Owens, Tyndall Air Force Civil Engineering Center

Summary

The goal of this project was to explore physics, materials and surface chemistry behind the polymer-based route towards creation of magnetic ceramic composites out of magnetic nanorods and nanofibers. We successfully developed the experimental protocol aimed to make mullite coating films with embedded magnetic inclusions. Electrospun mullite nanofibers with incorporated magnetic nanoparticles, SiC whiskers decorated with magnetic nanoparticles, and Nickel nanorods were successfully embedded into mullite films. We developed an experimental procedure guarantying the reproducible preparation of magnetic silicon carbide (mSiC) whiskers for the use as fillers in the mullite based composite films. We studied kinetics of collective alignment of nanorods and fibers in mullite precursor undergoing a sol/gel transition under uniform magnetic field. These studies resulted in a successful development of the experimental protocol for controlled alignment of nanorods/nanofibers in thin films prior to the complete solidification of the film. We also studied the mechanisms of nanorod-nanorod interactions in non-uniform magnetic fields and developed a robust procedure to control the nanorod placement using a non-uniform field with a designed gradient. Crack-free magnetic composite films with mullite matrix have been synthesized and characterized. Fifteen papers were published based on the results of this project. In 2013, a PhD student, Yu Gu, who worked on this project, was awarded the First Prize in the student paper competition of the Fiber Society. Mr. Zhaoxi Chen was selected to receive the 2015 Hitachi High Technology Electron Microscope Graduate Fellowship and will continue working on this project studying magnetic phase transformations in nanorods and nanoparticles embedded in mullite film. Two PhD students, Yu Gu and Maryana Nave successfully graduated with the PhD degrees. Thus, the project was scientifically and academically successful.

Table of Contents

1 Specific tasks

The research program has been structured to address the following challenges

(1) Synthesis and surface modification of Ni nanoparticles and nanorods;
(2) Development of experimental protocol for alignment of magnetic nanorods in solidifying films.
   a) Theoretical analysis of effect of the film viscosity; nanorod magnetization, and strength of magnetic field on kinetic of alignment of an assembly of magnetic nanorods
   b) Experimental studies and optimization of process parameters to control the nanorod alignment in the film.
(3) Synthesis and surface modification of SiC nanorods decorated with magnetic particles
   a) development of the experimental procedure for reproducible preparation of magnetic silicon carbide (mSiC) whiskers for the use as fillers in mullite based composite films
   b) their initial incorporation into the mullite matrix.
(4) Development of the electrostatic spinning of nano and micro fibers as possible candidates for fillers in ceramic-ceramic composites.
   a) Formulation of the spinning dopes,
   b) Synthesis of magnetic ceramic-based nanofibers
   c) Development of characterization methods to probe mechanical properties of electrospun nano and microfibers;
(5) Study the evaporation kinetics of ceramic precursors;
(6) Design of the experimental protocol to fabricate defect-free ceramic coatings.

1.1 Synthesis and surface modification of nickel nanoparticles (NiNP)

Nanoparticles. NiNP were chosen because of their attractive magnetic properties and availability on the market. However, we found that the specifications of the purchased particles do not match the values claimed by the manufacturers: impurities, average particle size and size distribution appeared wrong. On contrary, there are several proven synthetic approaches to prepare NiNP, which allow synthetic flexibility, good control and reproducibility of the particle properties. Therefore, in our studies we focused on the synthesis of NiNP by reduction of nickel chloride with hydrazine in the presence of sodium hydroxide [1]. Depending on the used media (ethanol or ethylene glycol) and the chosen concentration of reagents, the desired size of the particles can be obtained. The purity, size and magnetic properties of NiNP prepared in our laboratory were evaluated using XRD, SEM/TEM and magnetometry. These NiNP were synthesized for incorporation into ceramic nanofibers or making magnetic chains in the presence of magnetic field.

The major challenge in preparation of magnetic precursors is the particles dispersibility and colloidal stability. To improve these qualities we performed the surface modification of the particles by grafting polymer layerson the NiNP surfaces. There is a limited number of publication

dealing with the alternation of the surface chemistry the ferromagnetic nanoparticles' [2-4]. In all these publications, the surface modification is specific to the environment/solvent. In contrast, to stabilize the particles against aggregation, we used polyethylene glycol (PEG) known for universal solubility/affinity to the solvents of various nature. As a result, significant improvement of the colloidal stability was observed in different solvents.

Nanorods (NiNR). Two different procedures where used in this task. NiNR were synthesized by electrochemical deposition [5] using alumina membrane as a template. To ensure uniformity of the dispersion, the surface of nickel nanorods was covered with polyvinylpyrrolidone (PVP) using the method developed in Ref. [6]. Considering economic factors (costly alumina templates and limited amount of the material synthesized per a single template) the second approach was developed. Nickel nanorods (NiNR) were synthesized by the reduction method used for NiNP synthesis. A higher temperature and smaller concentration of Ni salt were chosen to fulfill the conditions favorable for nanorod formation [7]. This synthetic templateless approach allows one to synthesize larger quantities of the material making it much more economically viable. Changing the experimental conditions one can obtain nanorods with different diameters and aspect ratios. Both types of nanorods were used in experiments on alignment of nanorods in magnetic field.

1.2 Development of experimental protocol for alignment of magnetic nanorods in solidifying films

The strategy for nanorod alignment in macroscopic materials has not been developed in the literature and this remains the main challenge in materials engineering and processing. This problem requires understanding the kinetics of alignment of an assembly of nanorods. It also requires the development of advanced physicochemical methods of nanorod stabilization against agglomeration. A 40–70 nm PVP coating prevents aggregation of nanorods dispersed in a water–glycerol mixture. An orientational distribution function of nanorods was introduced and then studied both theoretically and experimentally. We also theoretically studied the kinetics of ordering of nanorods suspended in a solidifying liquid film. This analysis of kinetics was very important for the fabrication of ceramic nanocomposites film.

1.3 Synthesis and surface modification of SiC nanorods decorated with magnetic particles

Axisymmetric nanofillers (silicon carbide whiskers) are inexpensive and readily available on the market [8]. Their mass-production has been already established for many years. Thus, the SiC whiskers are naturally considered as a suitable candidate for nanofiller.

Incorporation of magnetic component into the whiskers is carried through reduction of poly(2-vinyl pyridine) (P2VP)-Ni complex [9] by hydrazine to pure metallic Ni. At first, the surface of the whiskers is modified with P2VP using poly(glycidyl methacrylate) (PGMA) as an anchoring layer [10] and "grafting to" approach [11]. Then, Ni-P2VP complex is formed in presence of Ni salt solution. Next, the reduction process takes place.

Though similar reduction technique was applied to prepare gold nanoparticles on the surface [12] it is for the first time that it is used to obtain nickel as well as decorate nanoobjects with nickel nanoparticulates.

Several methods of creating magnetically orientable nanofillers for composite films (chains of Ni nanoparticles, Ni nanowires) have be proven achievable in our laboratory settings but practical larger scale fabrication of those materials remained challenging. To this end, (commercially available) SiC whiskers decorated with (commercially available) magnetic iron oxide nanoparticles were suggested as magnetically active composite filler. The components of the mSiC system are inexpensive justifying their practical usage for fulfillment of the project's goals.
The experimental procedure to fabricate mSiC was developed in our laboratory and consists of:

1. cleaning of SiC whiskers by heat treatment (400 ^{o}C, air);
2. size selective separation of the whiskers by combined multiple sedimentation and centrifugation procedures;
3. surface modification of SiC whiskers with epoxy silane;
4. surface modification of epoxydized whiskers with poly(2-vinylpyrydine) (P2VP);
5. purification of iron oxide nanoparticles by multiple centrifugation to isolate the smallest (10-20 nm) particles;
6. surface modification of the particles with polyacrylic acid (PAA);
7. decorating of the whiskers with the nanoparticles through the formation of insoluble P2VP/PAA complex resulting in mSiC;
8. final coverage of the mSiC with PAA nanoscale layer to achieve good dispersibility in methanol and water media (the same media used to dissolve mullite precursor).

Figure 1 illustrates the principal scheme for preparation of mSiC whiskers described above. The developed methodology allows achieving flexibility in final magnetization of the whiskers through adjusting magnetic nanoparticles to the whiskers ratio.

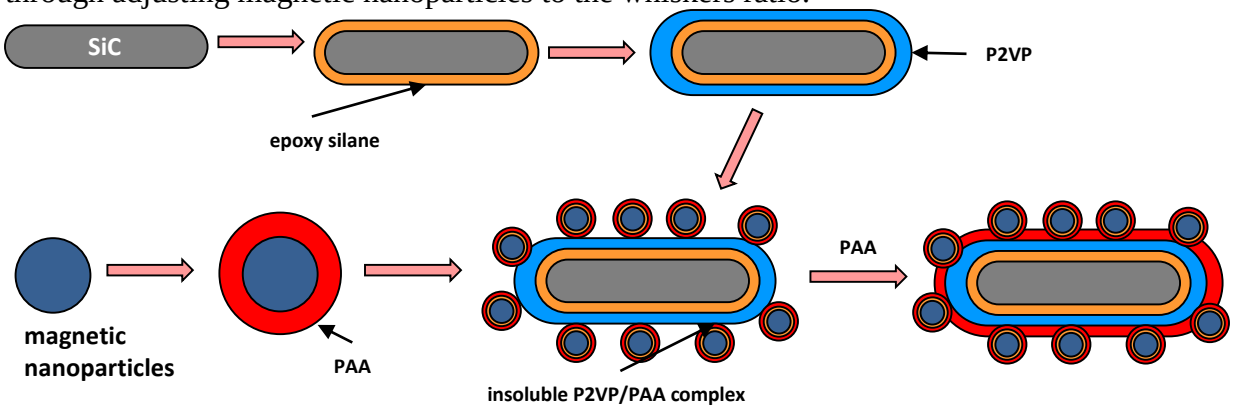

Figure 1. The scheme of the fabrication of mSiC whiskers.

1.4 Development of the electrostatic spinning of nano and micro fibers as possible candidates for fillers in ceramic-ceramic composites.

Electrospinning of mullite nanofibers has been previously studied by other researchers [13, 14]. However in these studies, the obtained nanofibers were produced in the form of a random fiber matt. Hence, one cannot use this method for further processing and formation nanocomposites

with aligned nanofibers. In our study, we focus on understanding of the mechanisms of nanofiber formation enabling precise control of the fiber diameters from nanometers to micrometers and the alignment during the fiber collection. Mechanical properties of nanofibers are known to depend on the fiber diameter. Available literature deals with mullite microfibers [15-18]; characterization of mechanical properties of nanofibers is seldom discussed in the literature [19-22]. Mechanical properties of electrospun ceramic nanofibers has never been discussed in the literature, hence we have been concentrated on the development of an experimental protocol to obtain these properties. For microfibers, the single filament tensile test was routinely employed to obtain the fiber strengths.

1.5 Processing mullite-nickel composite fibers using the *in-situ* reduction method

Magnetic mullite fibers have never been reported. To fabricate magnetic mullite fibers, two synthesis strategies were used. In the first strategy, we synthesized nickel nanoparticle coated with polymer, and then grafted the nickel nanoparticle on the fiber surface. In the second strategy, we introduced Ni nanoparticles by reducing nickel oxide in the amorphous mullite fiber preforms at different temperatures in hydrogen. The Ni nanoparticles must be precipitated within the fiber at low temperatures before mullite phase is formed at the high temperatures. Otherwise, nickel oxide will react with the alumina to form nickel aluminate spinel. Once this spinel phase is formed, it is impractical to eliminate this phase. The size of the nickel nanoparticles can be controlled from blow 10 nm to above 50 nm, by using different reducing temperatures and nickel contents. The fiber magnetic property relates to the microstructure.

1.6 Evaporation kinetics of mullite precussor

To fabricate the Mullite composite coatings with ordered magnetic structure, we have to first understand the evaporation kinetics of the mullite precussor. Following the theory developed for alignment of nanorods in solidifying film, we must ensure the complete alignment of nanorods before the solidification of film [23]. To fully understand the evaporation process, we studied both the mass loss and viscosity change for evaporating precussor. Cahn DCA-322 Analyzer was used to measure the mass loss during the evaporation of a mullite film. A quasi-static model developed in Ref[24] was applied to extract the characteristic time of evaporation. Magnetic Rotational Spectroscopy (MRS) was used to study the viscosity change[25]. The viscosity is proved to be exponentially increasing during evaporation.

1.7 Design of the experimental procedure to fabricate defect-free mullite coatings

In order to process the composite coatings with oriented nanowebs, we need to understand the processing of mullite coatings. We studied the conditions of forming mullite coatings. Several studies show that deposition of mullite using the sol-gel precursor is possible, but always accompanied with cracks [26, 27]. The probability of crack formiation depends on the residual stress in the film. The critical thickness, a maximum thickness of non-repetitive deposition above which the cracking occurs, is an important characteristic of sol-gel coating process. Usually sol-gel coating process results in small critical thickness, above which cracking and decohesion cause problems. In this study we use mullite prepared by sol-gel dip coating as an example system to understand the effect of polymer additives on the coating's critical thickness. Mullite thin films

were prepared from a monophasic sol-gel precursor. In our research of processing mullite films, poly(ethylene oxide) (or PEO), polyvinyl alcohol (or PVA) and polyvinylpyrrolidone (or PVP) were added in the precursor to prohibit the crack formation. Mullite coatings with different thickness were obtained by the dip-coating method with different pulling rate. Multi-layered mullite coatings were processed in order to achieve thick crack-free mullite films. Multiple coating was also done to study the healing mechanism of cracked thick films by repeated deposition.

1.8 Synthesis of ceramic films with aligned magnetic nanorods

In this task, we addressed the following objectives: 1) to demonstrate ordered magnetic microstructure embedded in ceramic coatings; 2) to study cracking behavior of ceramic coatings over pre-fabricated structures using dip-coating method; 3) to control magnetic particle precipitation with ceramic fibers. Two approaches were used to embed ordered magnetic microstructure in ceramic coatings as shown in Fig 2. In the first approach, magnetic Ni and mSiC nanorods were deposited on a substrate from a polymer solution. After their alignment as discussed in Refs. [28-30], the polymer was subsequently removed and the nanorods were sintered on the substrate. In the second approach, mullite nanofibers were electrospun and aligned during the spinning process. The alignment was achieved with an electric field-assisted alignment technique using split counter-electrodes. Nanofiber arrays were collected on silicon substrates. The fishnet fiber structures were obtained with multiple layers of aligned fibers. The as-spun fiber arrays were heat treated in reduced atmosphere in order to precipitate the Ni magnetic nanoparticles from the host mullite fibers. Then a layer of mullite coating was achieved using sol-gel/dip-coating method.

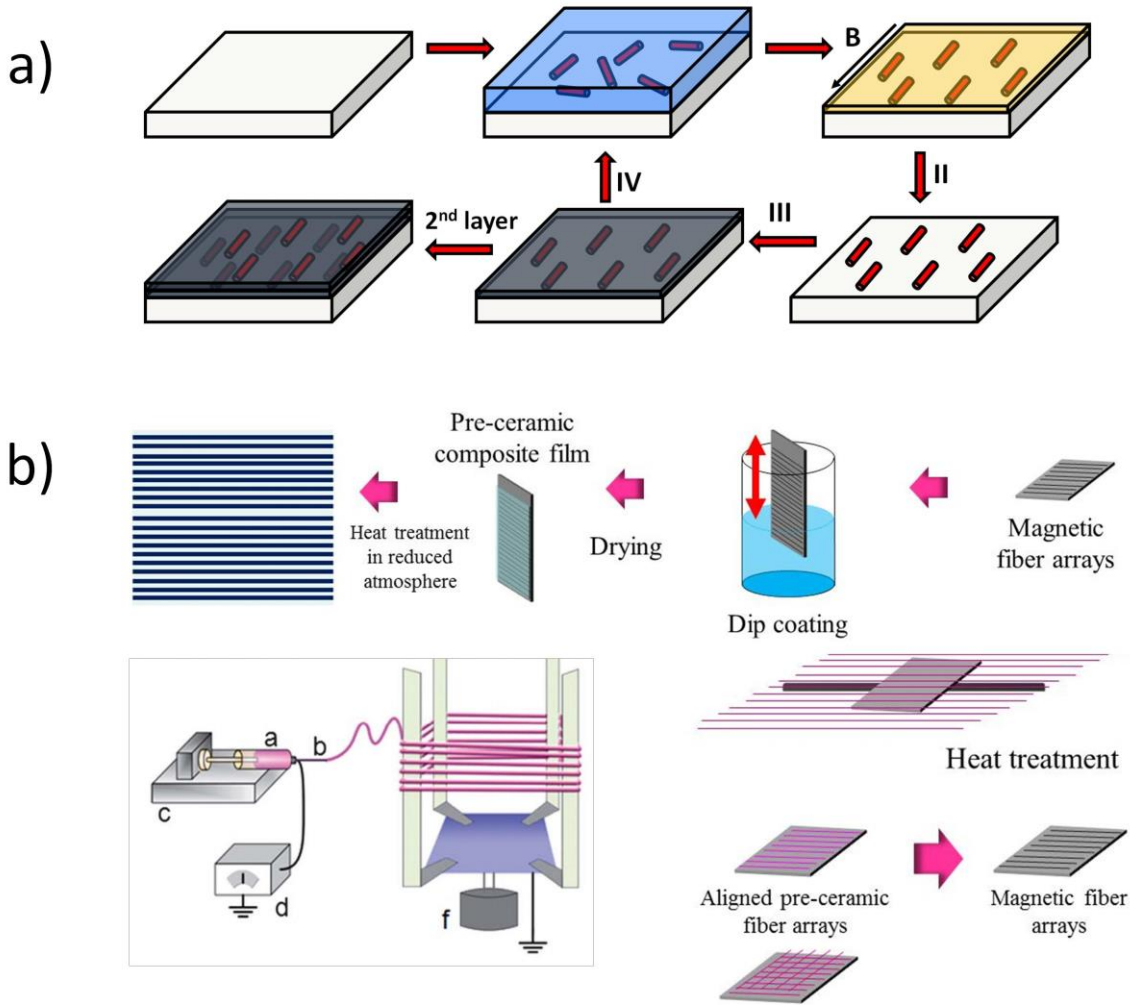

Figure 2. a) magnetic nanorods were first deposited on a substrate from a polymer solution and then aligned in the polymer film. The polymer was removed and nanorods were fused to the substrate during the heat-treatment. Ceramic coating was processed on the top of the aligned nanorods. b) Ceramic fibers were electrospun on the substrate with alignment enabled by the electric field. Magnetic nanoparticles were precipitated within ceramic nanofibers Ceramic coating was then processed on the top of aligned nanofibers.

2 Main findings

2.1 Nickel nanoparticles and nanorods

The size of Ni nanoparticles synthesized in our laboratory was found to be about 100 nm (Figure 3). By adjusting experimental conditions it is possible to prepare smaller size particles as well.

The particles were successfully modified sequentially with PGMA and PEG polymer layers (Figure 4). The thickness of PEG layer is 10±2 nm (Figure 4b). The dispersibility of the NiNP in water, ethanol or even toluene was improved significantly after the polymer grafting.

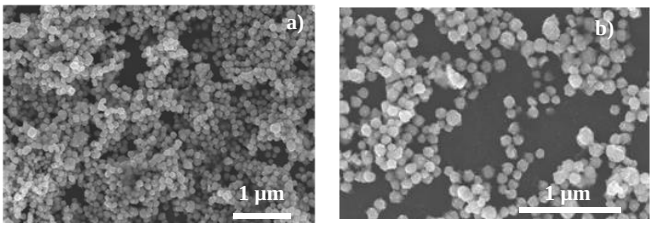

Figure 3. SEM images of as synthesized NiNP a) lower and b) higher magnification.

The 100 nm Ni nanoparticles are composed of pure metallic nickel and are ferromagnetic (saturation magnetization - 30 emu/g, coercivity -90 Oe) as confirmed by the XRD and magnetometry measurements.

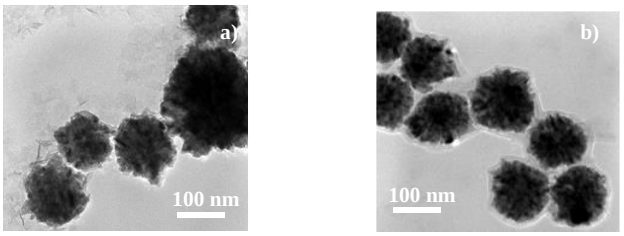

Figure 4. TEM images of a) original and b) surface modified NiNP.

These NiNP demonstrate very interesting behavior in magnetic field. Namely, original "as synthesized" nanoparticles and modified ones in the presence of external magnetic field readily form chains. However, whereas "original" chains are completely rigid and do not change their configuration in the absence of magnetic field, the "modified" chains possess extremely high degree of flexibility and at zero field can attain "globular" structure of completely collapsed chains (Figure 5a,b). This transition is completely reversible and chains are formed again upon application of the external field. Even more visually stunning example of this phenomenon was observed for multilayer large chains formed of modified nanoparticles (Figure 5c, d). The chains can fold on itself to the highest degree attaining a "snake-like" configuration. It is for the first time that such effect was demostrated for magnetic nanoparticles.

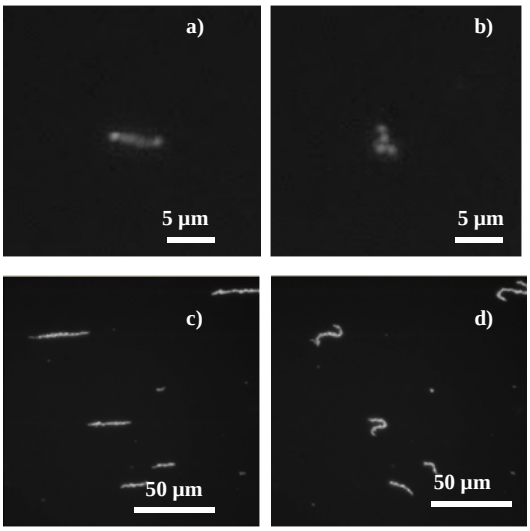

Figure 5. Dark-field optical microscopy images of NiNP short (a,b) and long (c,d) chains with magnetic field on (a,c) and off (b,d).

NiNR synthesized by electrochemical technique was found to be ferromagnetic and of pure metallic nickel. After the surface modification [10] the rods are covered with stabilizing PVP layer (Figure 6a). They align in magnetic field, but in order to achieve high concentration of the rods and at the same time avoid aggregation, the viscosity of the media (the rods are dispersed in) should be much larger than that of water. With the purpose to elucidate the possibility of NiNR alignment in ceramics a series of experiments were performed using actual Mullite precursor solution (40 wt.%). Despite very high concentration, a large amount of water still had to be removed from the solution to achieve the higher viscosity. Combination of high viscosity and high concentration of well-dispersed nanorods resulted in successful embedding of magnetic nanofillers into the partially dry film of Mullite (Figure 6b).

Typical NiNRs formed in the reaction bath have about 150 nm in diameter and about 3-5 µm in size (Figure 6c). The rods are composed of NiNP fused together. In initial experiments, the nanorods produced by this method were dispersed in 4 wt.% of PVP to increase viscosity of the solution and improve dispersibility of the nanorods. The nanorods demonstrating very good alignment (Figure 6d).

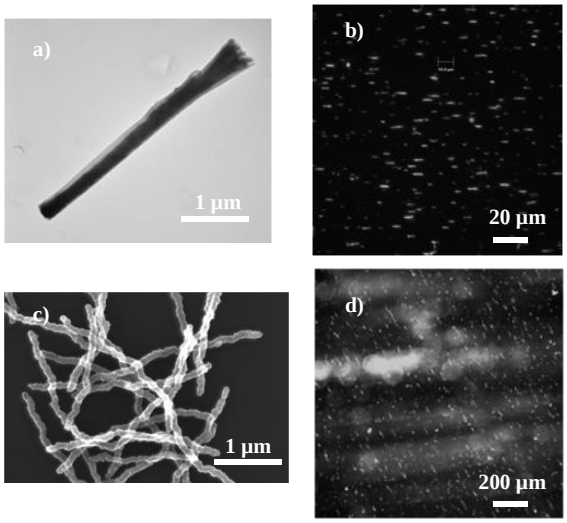

Figure 6. SEM (a,c) and dark-field (b,d) images of NiNR (a,b) and tNiNR (c,d)

2.2 Collective alignment of Ni nanorods under uniform magnetic field

Nickel nanorods were formed by the template electrochemical deposition in alumina membranes. To ensure uniformity of the dispersion, the surface of the nickel nanorods was covered with polyvinylpyrrolidone (PVP). A 40–70 nm coating prevented aggregation of nanorod. These modifications allowed us to control alignment of the nanorods in a magnetic field and test the proposed theory. An orientational distribution function of nanorods $F(\varphi,t)$ was introduced to characterize the alignment of Ni nanorods assembly. The angle φ indicates the direction of nanorods. We demonstrated that the 0.04% volume fraction of nanorods in the glycerol–water mixture behaves as a system of non-interacting particles. Starting from a random distribution, the time evolution of this function is written as:

$$F(\varphi,t)=\frac{1}{2\pi}\frac{2C}{(C^2-1)\cos\varphi+(C^2+1)} \qquad (1)$$
$$C=\exp(-\beta t)$$

$\beta=mB/\gamma$ is the physical parameter of the system and $1/\beta$ is the characteristic time for the alignment of nanorods.

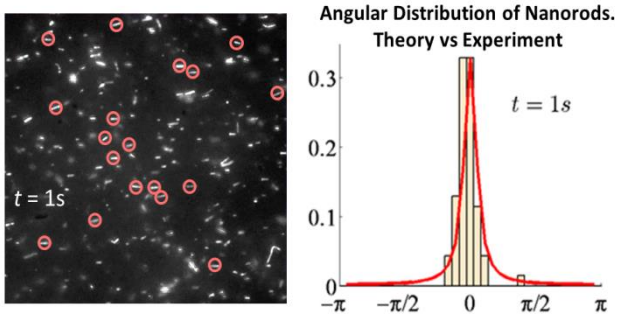

Figure 7. The angular distribution function of nanorods at t=1s. Experimental image and theorical fitting.

As shown in Figure 7, we can take a snapshot at a certain moment and estimate the distribution function from the image to produce a histogram. The theoretical results (red line) calculated from eq.(1) fit well with the experimental data.

We theoretically predicted and experimentally confirmed that one can control the alignment of an assembly of nanorods by choosing the parameter β and time of application of the external field. To better model the process of alignment of nanorods in ceramic films, we theoretically calculated the time evolution of distribution function in solidifying film. Assuming random orientation of nanorods at the initial moment of time, we estimated the time needed for nanorods to align along the direction of external magnetic field. In the solidifying films with exponentially increasing viscosity ($\eta=\eta_0 e^{t/\tau}$), the viscous drag significantly resists the nanorod alignment. Therefore, some nanorods might be quenched halfway to the equilibrium orientation even before complete solidification of the film. Figure 8 shows the alignment of nanorods when film is completely solidified. To achieve complete alignment, one has to decrease U_0 as much as possible. To do that, we can decrease the initial viscosity η_0, decrease the evaporation rate (making higher τ) or apply stronger magnetic field B.

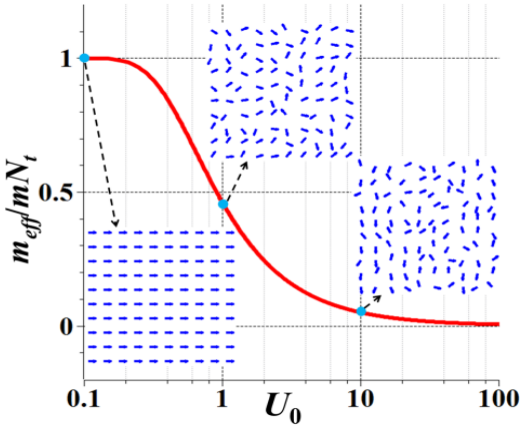

Figure 8. Final configuration of nanorods as a function of initial condition. U_0 is the physical parameter proportional to the ratio $\eta_0/(\tau mB)$.

Many-body interactions and classification of possible phases offered by magnetic suspensions attract significant attention in the materials science community [31-40]. The shape of magnetic particles becomes very important in this respect because it affects the way of particle packing and their magnetic order in the condensed phase.

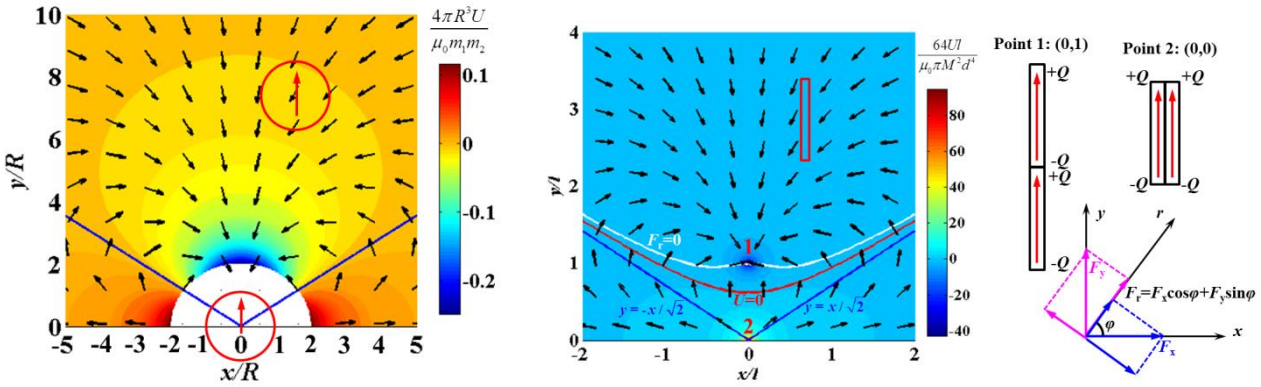

Figure 9. a) Landscape of the energy of interactions between two magnetic nanobeads with parallel magnetic moments. One is fixed at the origin, the other is free to move (it is circled in this picture). The color bar specifies the strength of the dipole-dipole interactions. The black arrows indicate the direction of the force acting on a mobile bead. The blue lines ($y=\pm x/\sqrt{2}$) corresponding to zero energy U=0 and zero x-component of the force, $F_r=0$, divide the diagram into zones of particle attraction and repulsion. b) Landscape of magnetostatic energy of two parallel nanorods with co-aligned magnetic moments. The white line ($F_r=0$) is the boundary separating the zones of nanorod attraction and repulsion. The red line is the line of zero energy (U = 0). The blue lines ($y=\pm x/\sqrt{2}$) are the boundary lines of the zones of attraction and repulsion for the beads (adopted from Refs. ***[41, 42]****).*

The shape of the interacting particles affects the magnetostatic energy of particle-to-particle interactions as well. Figure 9 shows the landscape of the interparticle energy U for two magnetic beads with magnetic moments m_1 and m_2 and radius R each. The white semicircle is the forbidden region for the incoming particle: the particle can only roll over the surface of the fixed particle and is not able to penetrate it. When the pair forms the head to tail configuration, the energy takes on its minimal value. In contrast, two magnetic nanorods of length *l*, diameter *d*, and magnetization *M* each, interact via their end poles [38, 39, 43]. Consequently, a weak dipole-dipole interaction of two beads, with the energy scaling as one over the distance cubed, is changed to a strong Coulomb interaction between magnetic "charges" ±Q, with the energy U scaled as one over the distance. As a result, the zone of repulsion for two parallel nanorods significantly increases as shown in Figure 9 b) with the white line [43]. This boundary separating the attraction and repulsion zones is specified by analyzing the radial component of the magnetic force $F_r = F_x \cos\varphi + F_y \sin\varphi$. If $F_r > 0$, the magnetic force tends to push the nanorods apart and the strongest repulsion occurs at point 2. If $F_r < 0$, the magnetic force tends to bring the nanorods together indicating an attraction. In a stable equilibrium configuration when the nanorods come together head to tail, point 1, the attraction is the strongest. The boundary separating the attraction zone from the repulsion zone is specified by the critical condition $F_r = 0$ (the white line in Fig. 9b). As the distance between the nanorods increases, this boundary shrinks and gradually merges with the blue lines ($y=\pm x/\sqrt{2}$) separating the attraction and repulsion zones of two dipoles. Hence, the behavior of nanorods becomes almost indistinguishable from that of spherical beads as the distance between them becomes much greater than the nanorod length.

The self-assembly of magnetic particles in dispersions reflects the specifics of their two-body interactions. The phase diagram for two nanobeads reveals a larger area of the attraction zone: where the nanorods of finite length repel each other, the nanobeads of the same magnetization can come together [43]. The self-assembly of magnetic beads in an external magnetic field often proceeds via formation of 1D (chains) to 2D (sheets) and then, even further, to 3D structures [44, 45]. Clusters of magnetic beads are very difficult to destroy[46-50], most likely, because even after removal of the external field, the dipoles self-support the structure due to their internal field[51].

In a non-uniform magnetic field, one more mechanism of nanoparticle clustering has to be considered. In order to construct the energy landscape for two nanorods, it is convenient to introduce a local system of coordinates (X,Y) where the center of coordinates at the center of mass of a reference nanorod is (0,0). In the vicinity of the central axis, the magnetostatic potential is represented as: $\varphi = -B_0 Y - \alpha(X^2 - 2Y^2)/4$, where B_0 is the constant component of a non-uniform external magnetic field at (0,0). As a measure of the strength of the field gradient with respect to the energy of mutual magnetostatic interactions between two nanorods, it is convenient to choose the ratio $\gamma = 4\pi L^2 \alpha/(\mu_0 Q)$, where L is the nanorod length, $Q = \pi d^2 M/4$ is the effective "magnetic charge" expressed through the nanorod magnetization M and its diameter d, $\alpha = -dB_Y/dY$ is the field gradient. When $\gamma << 1$, the field gradient has almost no effect on the incoming nanorod, and the two nanorods interact as if there were no field gradient. If this parameter is large, $\gamma >> 1$, the incoming nanorod should not feel any presence of the neighbor nanorod and, henceforth, it should be able to pass a fictitious boundary.

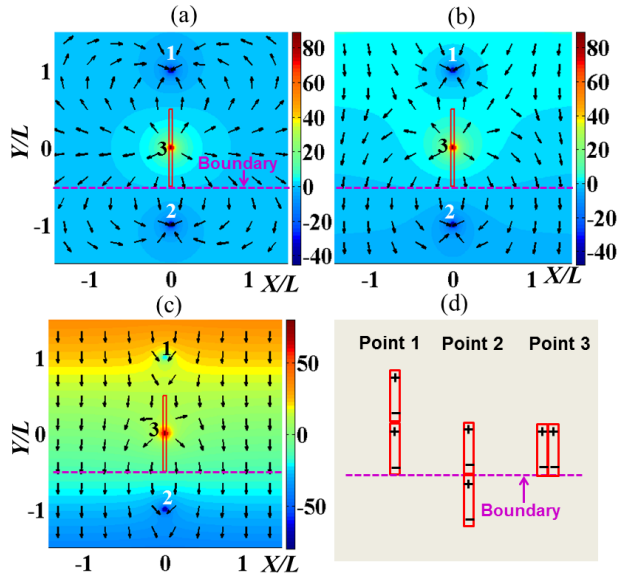

In the absence of an external magnetic field gradient $\gamma = 0$, the nanorods tend to come together forming a head-to-tail configuration Fig. 10(a). This case corresponds to points 1 (0, 1) and 2 (0,-1) in Fig. 10 (d) providing the same energy level.

Figure 10. The energy landscape for an incoming nanorod positioned at (X, Y). The reference nanorod has the same magnetization, length, and diameter. (a) The energy landscape for a nanorod subject to the field generated by the reference nanorod when the external field is not applied, $\boldsymbol{\gamma}$ =0. The reference nanorod is fixed to a fictitious boundary, the dashed purple line. (b) Deformation of the energy landscape caused by the field gradient corresponding to $\boldsymbol{\gamma}$ =2.5 (c) Effect of a strong gradient $\boldsymbol{\gamma}$ =25. Different colors represent different energy levels. The black arrows show the direction of magnetic force acting on the incoming nanorod. (d) In the absence of external field, configurations 1 and 2 correspond to the energy minima, and configuration 3 corresponds to the energy maximum.[42]

This analysis suggests that the nanorods can be effectively gathered into a cluster and moved to the required location by increasing the field gradient. The same idea works for spherical nanoparticles [52], Fig.6 a)-d). By applying the field gradient, one can gather magnetic beads into chains of different length and bring these chains to the given location. Figure 11 illustrates this effect on the locking magnetic nanoparticles (LMNP). These nanoparticles can be locked in place as soon as they come into contact with each other. Therefore, when the field gradient forces the particles to move to the substrate (at the bottom of Fig.11), they meet each other in the bulk, make bridges, and, finally, come to the given location as solid chains. Again, choosing a special field gradient, one can force the chains to build a forest placing chains next to each other.

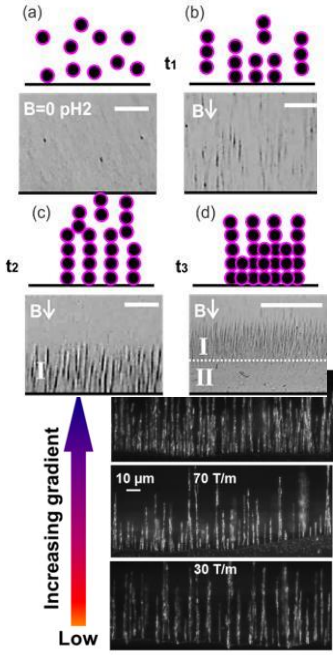

Figure 11. Snapshots and schematics of the formation of a chain forest using the field gradient. Concentration of LMNPs the electrolyte is 0.8 g/l, the field direction is shown by the arrows; Scale bars are 100 μm for all images: a) No aggregation was observed prior to application of the magnetic field at pH 2; b) When the magnetic field is applied, one can observe the formation of short chains in the bulk of the liquid; c) Chains move to the substrate and form a forest-like structure; d) The forest grows via formation of two distinct layers: the first layer is a low density layer of chains landing on top of the chains sitting in the second layer that is formed by a high density forest of magnetic chains. The layers are separated by a distinguishable boundary showed as the dashed line [52]. e) Effect of the field gradient on density of a forest made of Ni nanorods[42].

In the future research, we will take advantage of this phenomenon to assemble magnetic particles and nanorods into clusters of different sizes and then print these clusters on demand.

2.3 Electrospinning and characterization of mullite nano- and micro-fibers

The mullite precursor for the fiber spinning and film coating was produced using the sol-gel process. The hydrolysis and polymerization processes are affected by the pH values of solutions. Through control of chemical environment, the obtained gel can be monophasic or diphasic. Upon heat-treatment, the gel underwent decompositions between 200 and 400°C, and devitrification at about 980°C. Below 980°C, the material was amorphous. Above this temperature, a pure mullite phase was observed.

Mullite nano- and micro-fibers were produced via electrospinning of the sol-gel precursors. The fiber continuity and diameter can be affected by many factors, such as the molecular weight of the polymer content in the precursor, fluid's surface tension, applied voltage, viscosity, and solvent evaporation rate. In our study, PEO was used as the spinning aid. PEO has a good solubility and stability in the water-based precursors, and can improve the fiber continuity. during spinning. In

other studies, polyvinylprrolidone (PVP) was used for electrospinning of mullite nanofibers [13, 14]. We found that the stability of PVP in water-based precursor is unsatisfactory. Sometimes precipitation occurred as manifested by the solution turbidity. As a result, the e-spun fibers were not uniform.

Using PEO additives, uniform fibers with diameters measured between 400 nm to 10 μm can be produced on demand. The lower the viscosity, the thinner the fibers. For each batch, the fiber diameter is fairly uniform, as shown in Figure 12. The fiber can also be semi-aligned during collection, as shown in Figure 12 (a). Due to this semi-alignment, the fibers are less entangled compared to the ones collected as a nonwoven mat. Single fibers can be picked from the obtained fiber bundle. The bundles can also be twisted into yarns.

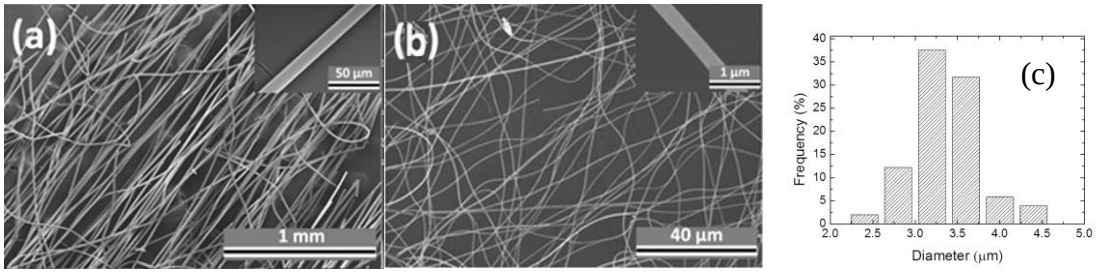

Figure 12. SEM micrographs of mullite nano- and micro-fibers after heat treatment in air at 1200°C. The diameters of the fibers are approximately (a) 10 μm, (b) 400 nm, (c) Statistical diameter distribution of mullite mico-fibers.

We studied the cross-sections of electrospun mullite fibers using SEM: no pores were observed inside fibers. The tensile strength was studied using a single filament tensile test. The mullite micro-fibers have very large tensile strength range. The tensile strengths for the 5 mm gauge length ranged from 0.99 GPa to 2.16 GPa, with an average of 1.46 GPa. The tensile strengths for 10 mm gauge ranged from 0.82 GPa to 1.90 GPa, with an average of 1.25 GPa. These values are comparable to the dry spun fibers [15-18].

2.4 Mullite-nickel composite fibers

To make fiber magnetic, nickel nanoparticles were introduced by first adding nickel oxide to amorphous mullite fiber preforms, and then reducing nickel oxide in hydrogen, followed by crystallization of mullite phase at high temperatures. Figure 13 shows the nickel nanoparticles formed within mullite fiber. The diameters of the nickel nanoparticles were from 10 nm to 50 nm.

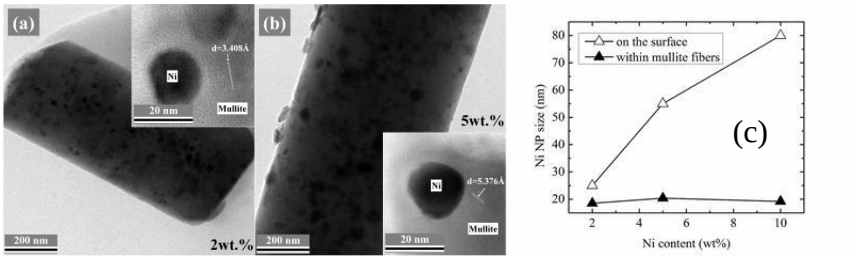

Figure 13. TEM micrographs of mullite-nickel composite fiber. (a) 5 wt.% Ni and (b) 2 wt. % Ni. (c) The Ni NP sizes on the fiber surface and within mullite vs. different Ni concentrations. The samples were heat-treated at the same temperatures.

After the Ni^{2+} was reduced to Ni NPs at 750°C for 10 h, the fibers were then directly transformed to the mullite fibers at 1000°C without the undesirable intermediate spinel phase. In many high temperature applications, mullite is the desired phase than spinel. If not fully reduced, the Ni^{2+} cations induce early precipitation of spinel phase before mullite can be formed. This spinel phase was a solid solution between Al_2NiO_4 and Al-Si spinels, which later reacted with the residual silica and formed a mixture of mullite and spinel at 1400°C. The formation of spinel phase was suppressed or fully eliminated with chemically reducing Ni^{2+} to metal NPs. The average size of nickel NPs within the fibers was ~20 nm, insensitive of the Ni concentration and reducing temperature. However the Ni NPs on the fiber surface grew as large as ~80 nm due to fast surface diffusion. The magnetic nanocomposites exhibited ferromagnetism with saturation magnetization (M_s) close to pure nickel of the same nominal weight, but coercivity (H_c) much smaller than the bulk nickel, indicating the nature of bimodal magnetic nanoparticle distributions. The majority of small Ni NPs (~20 nm) within the fibers exhibited superparamagnetism, while the minor portion of relatively large NPs (50 - 80 nm) showed ferromagnetism.

The magnetic properties of the obtained composite fibers are reported in Figure 14. Notable hysteresis was observed for 5% (MN5-750R-1000) and 10% (MN10-700R-1000 & MN10-750R-1000) Ni loaded samples indicating ferromagnetism. With the increasing temperature for thermal reduction, significant increase in M_s was observed, which implied a greater portion of Ni^{2+} cations were transformed into the metallic form. The H_c value increased with

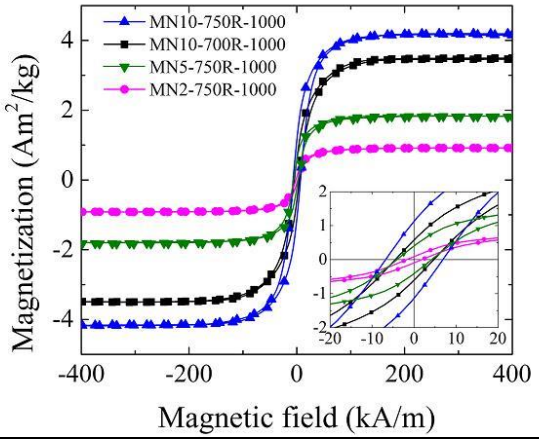

Figure 14. Hysteresis loops of mullite-nickel composite fibers after heat treatment in 5% H_2-Ar at 700 or 750°C for 10 hours, followed by heat treatment at 1000°C.

increasing Ni concentration and temperature for thermal reduction, which implied greater particle size of Ni.

2.5 Measuring flexural rigidity of mullite microfibers using magnetic droplets

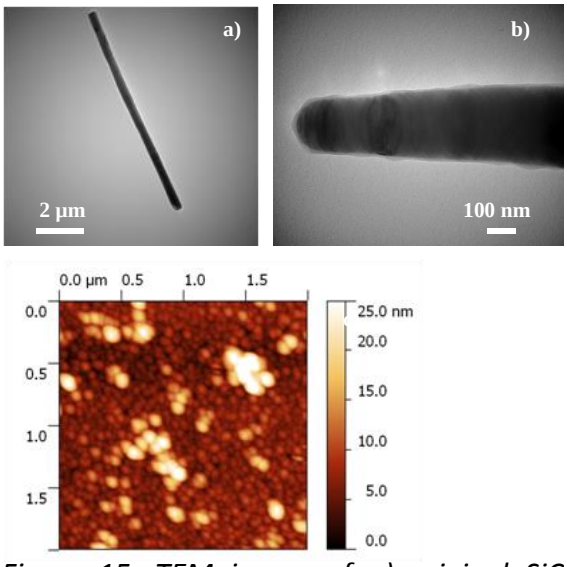

Figure 15. TEM image of a) original SiC whiskers, b) modified whiskers and c)AFM image of P2VP surface after reduction of the Ni complex.

We examined mullite microfibers formed by electrospinning of sol-gel precursors. The formed fibers had diameters smaller than 10 µm. A magnetic drop was placed on the free end of a dangling fiber and the fiber was flexed by applying a non-uniform magnetic field. By applying different magnetic fields, we generated a series of different fiber profiles and filmed the process of fiber bending. Mullite microfibers were found to follow the Bernoulli-Euler predictions and the shear deformations in the material were insignificant. This was confirmed by employing the Euler elastica model to describe the fiber profiles. The bending test provided a Young modulus of E =100 GPa which appeared to be very close to that found from the tensile test.

2.6 Magnetic SiC whiskers

The whiskers were purchased from Advanced Composite Materials LLC. The size of the whiskers is 400-500 nm in diameter and 10-12 µm in length (Figure 15a).

The successful modification with P2VP was confirmed by TEM imaging (Figure 15b). In addition TGA measurements showed decrease in weight of the fibers during the heating manifesting the presence of polymer layers (bare whiskers do not lose weight).

Formation of Ni on P2VP surface was studied using model P2VP layer grafted to silicon wafer using the same procedure as for the modification of the whiskers. The Ni absorption (in ethanol) and reduction (in ethylene glycol) was carried out at 60-70 ^{o}C [9] and 60 ^{o}C [53], respectively. The reduction resulted in nanoparticles formation on the P2VP surface as confirmed by AFM imaging (Figure 15c).

The morphology and for the typical mSiC is presented in

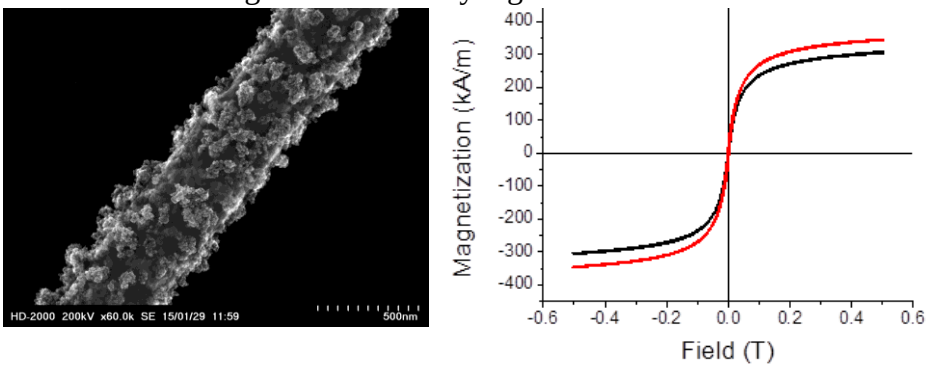

Figure 16. *a) SEM image of mSiC whisker (10:1 SiC whiskers to magnetic nanoparticles ratio) and b) magnetization curves of the mSiC whiskers.*

Figure 16 (a). The whiskers were found to be magnetic (Figure 16 (b)) and at the same time possessing good dispersibility and minimal to none tendency to aggregation. They also can be efficiently oriented in magnetic field.

2.7 Kinetics of Evaporation of the Mullite precursor

Mass change during evaporation of a Mullite precursor film is measured using Cahn DCA-322 Analyzer. Figure 17 shows that the theoretical model fits well the experimental data. The evaporation is a diffusion controlled process and evaporation rate is determined by the equilibrium humidity of the precursor P_w and ambient humidity P_0. From the fitting, we extracted the characteristic evaporation time τ and mass of the solute m_g.

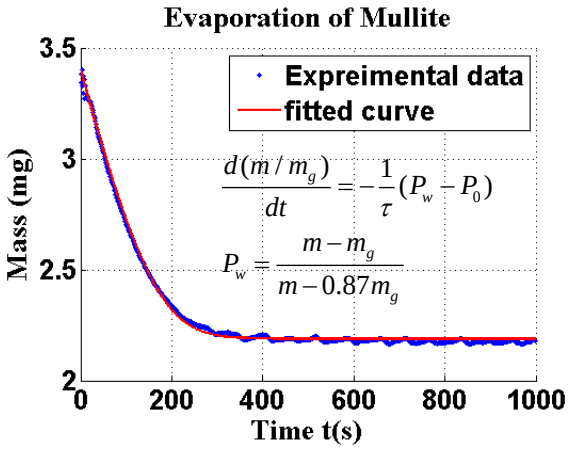

Figure 17. Mass loss with time during evaporation of Mullite precursor film.

Using MRS protocol to measure the viscosity in an evaporating film is very challenging especially when film is very thin. As a starting point, we investigate a Mullite precursor droplet. As shown in Figure 18, viscosity of an evaporating droplet increases exponentially with time. On the other hand, viscosity appears to be a function of concentration of Mullite and the increasing rate is closely related to the evaporation rate of the precursor. To ensure the complete alignment of nanorods before solidification, one can control the viscosity changes by controlling the evaporation rate through relative humidity P_0 or temperature.

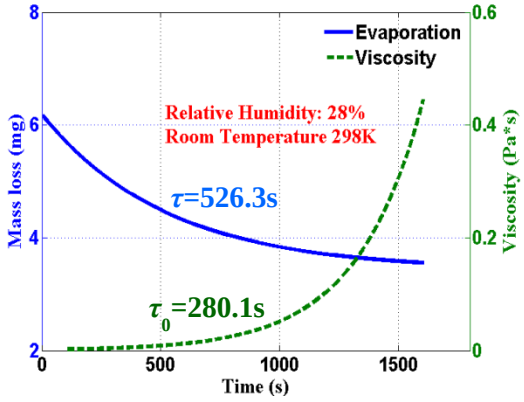

Figure 18. Mass loss with time during evaporation of Mullite precursor droplet and the corresponding viscosity increase.

2.8 Defect-free Mullite coatings

The maximum film thickness of non-repetitive deposition above which the cracking occurs is often termed the "critical thickness" (τ_c). For the sol-gel derived ceramic coatings, the τ_c value is typically below 100 nm. We used mullite films prepared from the monophasic sol-gel precursors as an example to study the effects of polymer additives on the coating critical thickness. The mullite and mullite-polymer hybrid gels demonstrated monophasic characteristics, enabling a low-temperature (1000°C) processing of nanocrystalline, phase-pure mullite films. The cracking in the films was only observed at the temperatures below 400°C as shown in Figure 19 (a). Increasing

the film thickness caused a decrease of the cracking onset temperature. Adding polymers, such as PVP, PEO, and PVA, in the precursor increased the critical thickness (Figure 19 (b)).

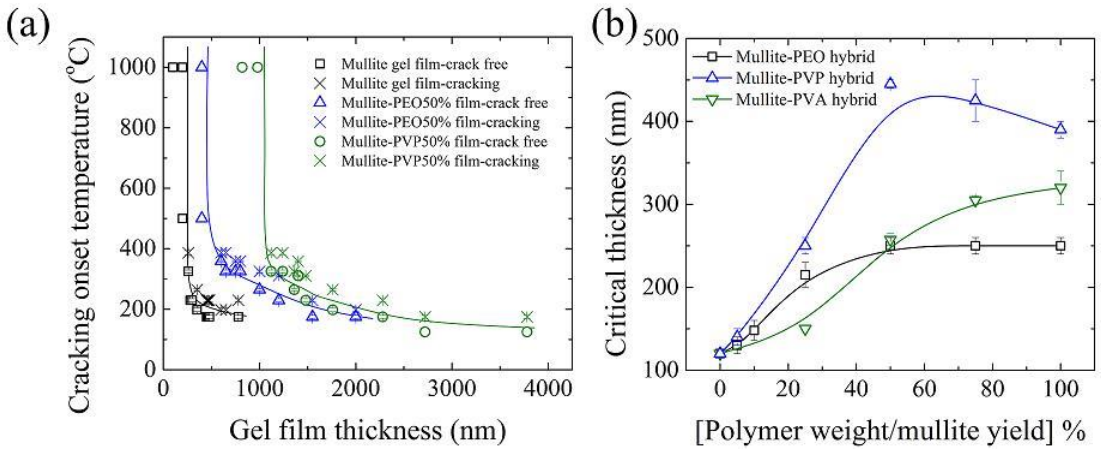

Figure 19. (a) Cracking onset temperature in mullite gel, mullite-PEO 50% and mullite-PVP 50% hybrid film (PEO: 50 wt. % of mullite yield and PVP: 50 wt. % of mullite yield) versus the gel film thickness. (b) Effect of polymer content on the critical thickness** of the hybrid films. (*: the thickness value is determined before firing; **: the thickness value is determined after firing).*

No further cracking was observed at temperatures higher than 400°C, indicating that thermal mismatch between ceramic coating and substrate did not significantly contribute to cracking. We thus conclude that cracking was mainly caused by the solvent evaporation during drying, the decomposition of polymer of organic component, and the densification during heat-treatment. The stress relaxation can be achieved by the viscous flow of polymers and the suppression of sol-gel polycondensation reaction with the polymer additives during drying and firing. After hydrolysis, the main condensation reactions in mullite can be described as follows [29]:

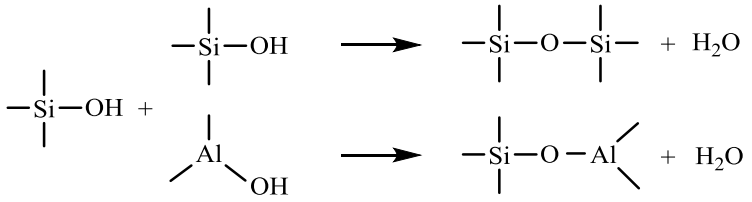

and,

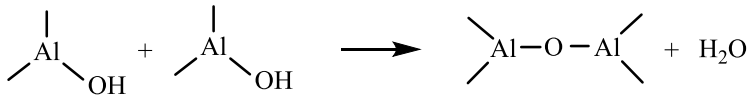

The carboxyl group in the polymer additives can react directly with the aluminosilicate sol to form a hybrid structure of metal-organic structure through the following chemical reaction, and thus retard the polycondensation process [54]:

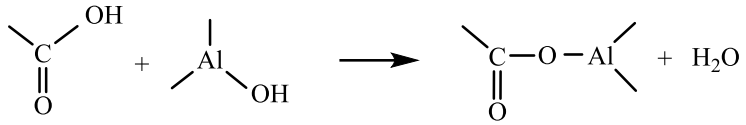

and,

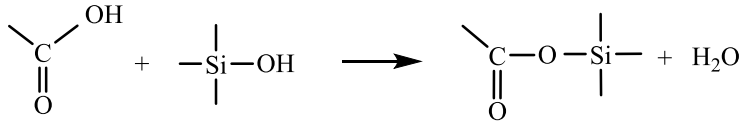

In Figure 20, the FTIR results showed the formation of C=O bonds up to 300 - 400°C in the coating with polymer additives such as PEO, PVP and PVA. Furthermore, PVP has better thermal stability than other polymers at this temperature, making it more effective in suppressing sol-gel polycondensation reactions than the other polymers.

Cracking at room temperature during drying can be effectively inhibited, even with addition of small amount of polymers. For instance, with the addition of 5 wt. % PEO of the mullite yield, the hybrid films were crack free during drying for the gel film thickness up to 2.5 μm. Further increasing polymer contents gave rise to even better cracking-resistant performance until an optimal concentration was reached. Although initially adding polymer resulted in greater critical thickness, an excessive amount of polymer could decrease the critical thickness, as shown in Figure 19 (b). The reason is that the gel volume was replaced by polymers, resulted in discontinuous oxide matrix after decomposition. The excessive porosity resulted in large intrinsic stress when solid was trying to densify driven by the capillary force.

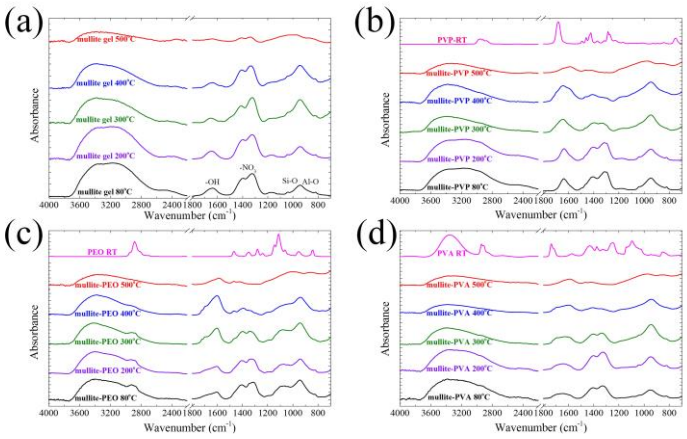

Figure 20. FTIR spectrum of (a) mullite, (b) mullite-PVP , (c) mullite-PEO and (d) mullite-PVA hybrid gel after heat treatment at 80(drying), 200, 300, 400 and 500°C. The polymer contents are 50 wt. % of mullite yield.

We attempted to heal the cracks present in thicker coatings by depositing several crack-free layers on top of it. The cracks

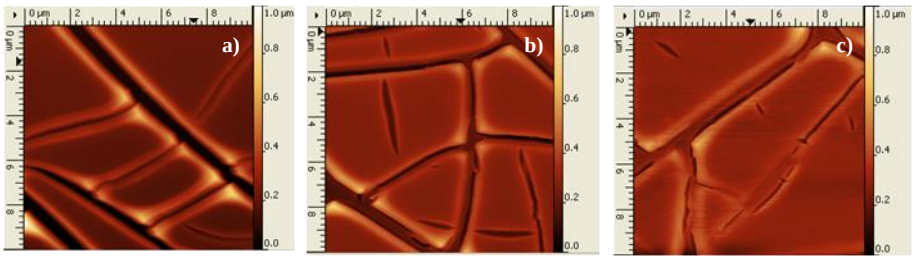

Figure 21. AFM images of Mullite coating a) original (150 nm), b) after 1st healing procedure and c) after 2nd healing procedure.

can be successfully healed (Figure 21) after several depositions. Roughly the same number of deposits were required to achieve the same final thickness of crack-free film as in the case of the layer-by-layer method. Considering similar work load of the two approaches studied the first one is preferred due to its higher consistency, reproducibility and ability to render crack-free film at any stage of the process.

2.9 The developed experimental protocol for creation of ceramic films with aligned magnetic nanorods

Taking into account the results described in the previous sections the final experimental protocol for incorporation of magnetic nanofillers into mullite coating and align them is based on layer-by-layer deposition and is as follows:

(1) Deposit layer of magnetic nanofillers (NiNR, NiNP, SiC whiskers) using high viscosity polymer solution (PVP, for example) incorporating the nanofiller.
(2) Align the fillers in magnetic field, dry the film and remove the polymer by decompoing polymer at high temperature (about 500 ^{o}C).
(3) Deposit a mullite precursor of the desired thickness by the layer-by-layer approach
(4) Repeat the process of sequential nanofiller-mullite deposition until the desired thickness is reached.

The descried process has a unique advantage. Namely, in the case of several' layers with nanofillers sandwiched in-between mullite layers the orientation of the filler in different layers can be different. It opens the door for creation closely spaced layers with perpendicular or any other orientation. It can be pushed up to the point where orientation changes gradually across the thickness of the coating. All this would be unique and achievable using just one magnetic material (nickel). The initial step of the preparation of mullite composite material in a thin film form is incorporation and alignment of the fillers in a polymer matrix followed by decomposition of the polymer and application of mullite coating. The fabrication of polymer composite films is a key stage in the overall process.

In our research, polyethylene glycol (PEG) was used as the polymer sacrificial material. The mSiC-PEG composite films were deposited onto silicon wafers by dip-coating technique. The samples were sealed in glass vial and exposed to the magnetic field immediately after deposition prior to crystallization of PEG that allowed orienting mSiC whiskers along the field. The sealing of the sample allows extending the time required to dry the film from 35s to 5 min. resulting in much better final alignment of the mSiC whiskers. The obtained composite material is presented in figure 22 (a). The efficient alignment of the whiskers is visible clearly, which is confirmed by

the quantitative analysis (figure 22 (b)). The prepared samples served as an excellent base for fabrication of ceramic composite films embedded with magnetic nanorods.

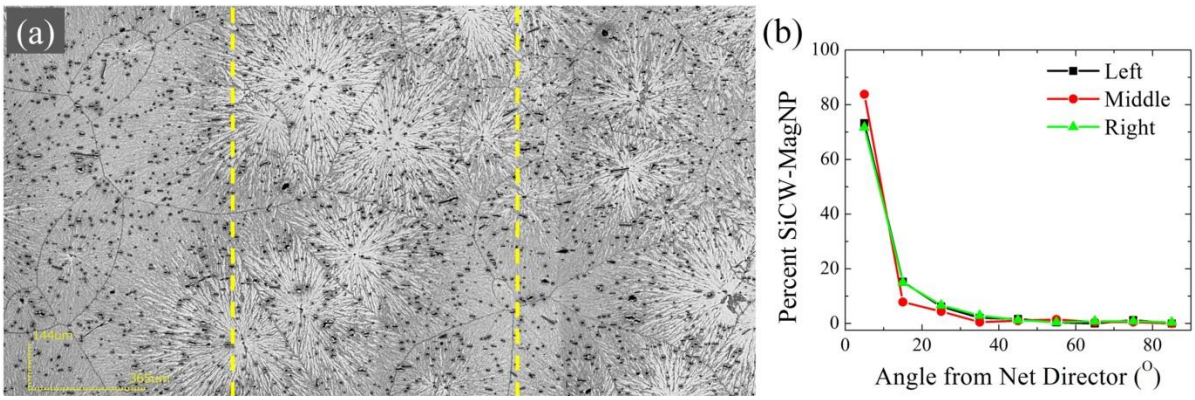

Figure 22. a) a stitched image of the composite thin film with 0.58%vol of SiCW-MagNP; b) the distribution of orientation from left, middle and right positions of the image

2.10 The developed ceramic films with aligned magnetic nanorods

Crack-free composite ceramic coatings have been successfully fabricated with embedded aligned magnetic nanorods or nanofibers as shown in Fig 23. The distribution of the SiC whiskers in polymer films, after polymer removal, after ceramic film deposition (before firing and after firing) is shown in figure 24. The nanorods/nanofibers retain good alignment throughout the process.

We studied the mechanism of crack formation in these composite coatings. The morphologies of mullite coatings with embedded nanofibers or nanorods can be divided into two categories as shown in Fig. 25. **Type 1:** When the critical thickness was greater than the diameter of the nanofibers or nanorods, no cracks were observed. Hereby, the critical thickness is the maximum thickness of ceramic coatings without cracking. Only a small protrusion on top of the nano-fibers/rods was observed on the surface of the coating using AFM. **Type 2:**

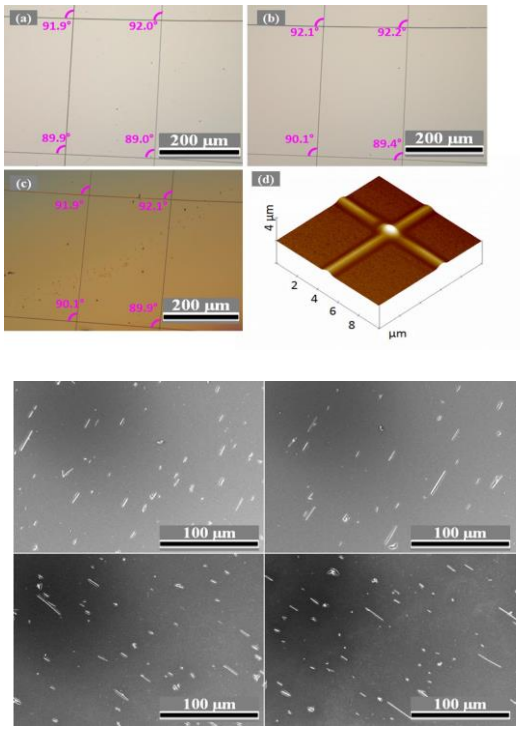

Figure 23. Ceramic coatings with embedded aligned magnetic nanofibers and nanorods: Top: mullite coating with embedded electrospun mullite fibers. Ni nanoparticles are embedded into these fibers. Bottom: mullite coating film with embedded aligned magnetic SiC nanorods.

When the critical thickness was smaller than the diameter of the nanofibers or nanorods. The cracks form when conformity of the coatings was poor. The film evolution in the vicinity of a nanofiber/nanorod can be categorized as conformal and planar profile. A conformal coating preserved the topographic feature of the substrate which showed no cracks. A planar coating, on the other hand, usually showed cracks, which had a substantial change of film thickness at the vicinity of nano-fibers/rods.

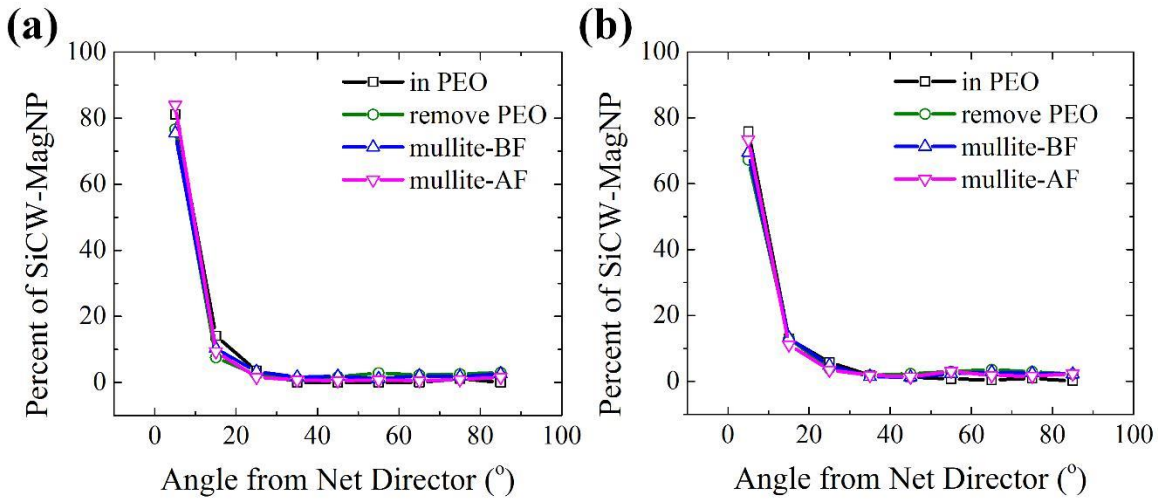

Figure 24. The distribution of orientation of SiCW. The initial concentration of SiCW in polymer films was 0.16 vol.% in (a) and 0.58 vol. % in (b).

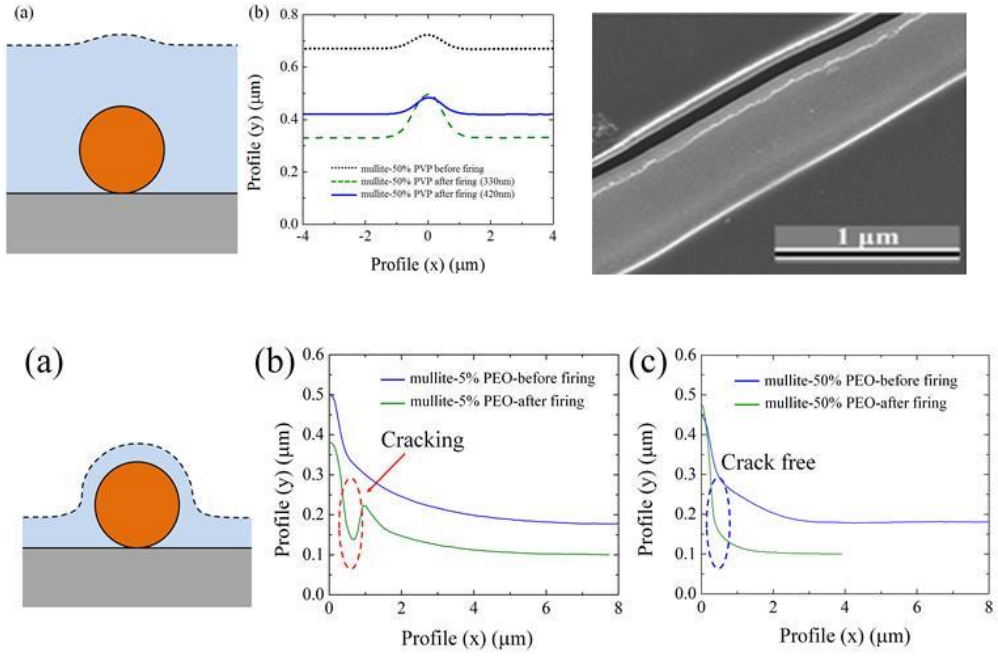

Figure 25. The two types of composite coatings. Type 1 is crack-free and was usually observed in thick mullite films (critical thickness ~ 400 nm) embedded with thin nickel nanorod (diameter ~ 200 nm). Type 2 composite thin film cracked after heat treatment when the surface profile showed a planar coating. The coating was crack-free after heat treatment for a conformal coating.

3 Publications/presentations/patents

3.1 Publications

1. Yu Gu and Konstantin G. Kornev, Alignment of magnetic nanorods in solidifying films, **Particle & Particle Systems Characterization**, DOI: 10.1002/ppsc.201300224 (2013)
2. Yu Gu, Ruslan Burtovyy, James Townsend, Jeffery R. Owens, Igor Luzinov, Konstantin G. Kornev, Collective alignment of nanorods in thin Newtonian films, Soft Matter, **Soft Matter**, **9,** 8532-8539 (2013) **(Editor's choice of "HOT PAPER" OF AUGUST 2013)**
3. Chen, Z., and Peng, F., "Normal and abnormal grain growths in BaTiO3 fibers." *Journal of the American Ceramic Society*, **97** [9], 2755-2761 (2014).
4. *Townsend, J, Burtovyy, R., Galabura Y., Luzinov I., Flexible chains of ferromagnetic nanoparticles* ***ACS Nano 2014, 8 (7), 6970-6978***
5. *Yu Gu, Zhaoxi Cheng, Nicolay Borodinov, Igor Luzinov, Fei Peng, and Konstantin G. Kornev, Kinetics of evaporation and gel formation in thin films of ceramic precursors,* ***Langmuir****, 30 (48), 14638–14647 (2014)*

6. *Yu Gu, Ruslan Burtovyy, John Custer, Igor Luzinov, Konstantin G. Kornev "A gradient field defeats the inherent repulsion between magnetic nanorods",* ***Royal Society Open Science****, 2014, DOI: 10.1098/rsos.140271*

7. *Alexander Tokarev , Yu Gu , Andrey Zakharchenko , Oleksandr Trotsenko , Igor Luzinov , Konstantin G. Kornev , and Sergiy Minko, Reconfigurable Anisotropic Coatings via Magnetic Field-Directed Assembly and Translocation of Locking Magnetic Chains,* ***Adv. Funct. Mater.*** *, 24(30), 4738-4745(2014),*
8. *Yu Gu and Konstantin G.Kornev, Attachment/detachment hysteresis of the fiber-based magnetic grabbers,* ***Soft Matter, 10****, 2816-2824 (2014)*
9. *Alexander Tokarev, Wah-Keat Lee, Igor Sevonkaev, Dan Goia, and Konstantin G.Kornev,*
10. *Zhaoxi Chen, Yu Gu, Zhao Zhang, Konstantin G. Kornev, Igor Luzinov, and Fei Peng, Measuring flexural rigidity of mullite microfibers using magnetic droplets,* ***Journal of applied physics*** *117, 214304 (2015).*
11. *Pavel Aprelev, Yu Gu, Ruslan Burtovyy, Igor Luzinov , and Konstantin G. Kornev, Synthesis and characterization of nanorods for magnetic rotational spectroscopy,* ***Journal of applied physics*** *118, 074901(2015).*
12. *Zhaoxi Chen, Zhao Zhang, Chen-Chih Tsai, Konstantin G.Kornev, Igor Luzinov, Minghao Fang, Fei Peng, Electrospun mullite fibers from sol-gel precursor,* ***Journal of sol-gel science and technology****, 74, 208-219(2015)*

13. Vladislav Vekselman, Luke Sande, and Konstantin G. Kornev, Fully magnetic printing by generation of magnetic droplets on demand with a coilgun, **Journal of Aapplied Physics** 118, 224902 (2015).
14. Chen Z, Gu, Y., Kornev, K., Luzinov, I., Chen, J., and Peng, F., "Mullite-nickel magnetic nanocomposite fibers obtained from electrospinning and thermal reduction", *Journal of American Ceramic Society*, DOI: 10.1111/jace.14148 (2016)
15. Gu Y. and Kornev K.G. Ferromagnetic Nanorods in Applications to Control of the In-Plane Anisotropy of Composite Films and for In Situ Characterization of the Film Rheology, **Advanced Functional; Materials,** DOI: 10.1002/adfm.201504205 (2016). **(Invited Feature Article)**

3.2 Presentations

[1] Townsend J., Burtovyy R., Luzinov I. "Modification of nanoparticles by grafting-to approach for flexible ferromagnetic nanoarrays" Ceramic, Composite and Optical Materials Center Meeting, Clemson, 2013.

[1] Chen Z, Peng F., "Electrospinning of Mullite and Silicon Carbide Fibers". *NSF IUCRC: Ceramic, Composite and Optical Materials Center Spring 2013 Industrial Advisory Board Meeting*, April 2013, Rutgers, NJ.

[2] Chen Z., Zhang Z, Kornev K., Luzinov I., and Peng F., "Mechanical properties of electrospun mullite fibers" *International Symposium on Fibers Interfacing the World*, The Fiber Society, 23-25 October 2013, Clemson, SC.

[3] Gu Y. & K.G.Kornev, Bending Hysteresis of Polymeric Fibers Caused by Micro- and Nano Newton forces, *International Symposium on Fibers Interfacing the World*, The Fiber Society, 23-25 October 2013, Clemson, SC***. THIS PAPER WAS AWARDED THE FIRST PRIZE IN THE FIBER SOCIETY STUDENT PAPER COMPETITION***

[4] Peng, F., "**Processing and Properties of Low-Dimensional Ceramic Materials**." invited presentation, Tsinhua University, Beijing, China; China University of Geosciences, Beijing, China; Shanghai Jiao Tong University, Shanghai, China; Shanghai Institute of Ceramics, Chinese Academy of Sciences, Shanghai, China, Dec 2014.

[5] Konstantin Kornev, Magnetic Rotational Spectroscopy with Nanorods for characterization of Rheology of Nanoliter Droplets and Sensing of NanoTesla Fields, **Magnetically stimulated soft materials, University of Georgia, May 11-12, 2015, Invited talk**

[6] Igor Luzinov *Flexible Chains of Ferromagnetic Nanoparticles,* **Magnetically stimulated soft materials, University of Georgia, May 11-12, 2015, Invited talk**

[7] Konstantin Kornev, Making thin magnetic multifunctional coatings, probing rheology of nanoliter droplets and thin films, making reconfigurable lattices, and printing magnetic materials on demand, Write-Patterson AFB, Ohio, August 5th, 2015

[8] Peng, F., Chen, Z., Kornev, K., Luzinov, I., and Xiao, H., **"Innovative mullite coatings with embedded magnetic nanorods**", MS&T 2015, Columbus, OH. Oct 2015. (**Invited talk**)

[9] Peng, F., Chen, Z., Kornev, K., Luzinov, I., and Xiao, H., "**Innovative mullite coatings with embedded magnetic Fishnet for the harsh environmen**t", MS&T 2015, Columbus, OH. Oct 2015. (**Invited talk**)

[10] James Townsend, Ruslan Burtovyy, Pavel Aprelev, Konstantin Kornev, Igor Luzinov. Magnetically responsive silicon carbide whiskers for nanocomposite materials, 251st American Chemical Society National Meeting & Exposition, Aug. 16-20 (2016), Boston, MA, USA.

[11] James Townsend, Ruslan Burtovyy, Pavel Aprelev, Konstantin Kornev, Igor Luzinov. Multifunctional silicon carbide whiskers for nanocomposite materials, 251st American Chemical Society National Meeting & Exposition, Aug. 16-20 (2016), Boston, MA, USA.

3.3 Patents

No patent has been applied.

3.4 List of honors

- Kornev K.G.: Outstanding faculty achievements in sciences, Clemson University, May 2013 (Highest recognition at the University level)
- Soft Matter Editor's choice of "HOT PAPER" OF AUGUST 2013)
- Yu Gu, PhD student supported by this grant, won the FIRST PLACE IN THE 2013 FIBER SOCIETY GRADUATE STUDENT COMPETITION
- Zhaoxi Chen, 'Hitachi High Technologies Electron Microscopy Fellowship' (2015)
- Luzinov, I. 2015 Outstanding Researcher of the Year (Clemson Chapter of Sigma Xi Research Society), April 2015
- Luzinov, I. The McQueen Quattlebaum Faculty Achievement Award that recognizes Clemson Engineering faculty accomplishments, April 2014

3.5 List of synergetic activities

Kornev K.G.: Chair of the International Symposium "Fibers Interfacing the World", 213 participants, 23-25 October, Clemson, SC, 2013
Fei Peng: Chair of Session: *Advanced Materials for Hash Environments*, MS&T 2015, Oct 4 - 8, 2015 (Columbus, OH).

Fei Peng: Chair of Session: *Nanotechnology for Energy, Environment, Electronics, and Industry*, MS&T 2015, Oct 4 - 8, 2015 (Columbus, OH).
Fei Peng: Chair of Session: Ceramic Fibrous Materials, at the Fiber Society Conference: International Symposium on Fibers Interfacing the World, October 23–25, 2013 (Clemson, SC).

4 Directions of the future research and challenges

(1) Develop mullite composite coatings with a 1D array of magnetic chains using layer-by-layer deposition technique.
(2) Develop methods of characterization of mechanical, magnetic, and optical properties of mullite precursors and composites.

5 References

1. Wu, Z.G., Munoz, M., and Montero, O. The synthesis of nickel nanoparticles by hydrazine reduction. Advanced Powder Technology *21*, 165-168.
2. Chen, R., Maclaughlin, S., Botton, G., and Zhu, S. (2009). Preparation of Ni-g-polymer coreâ€“shell nanoparticles by surface-initiated atom transfer radical polymerization. Polymer *50*, 4293-4298.
3. Rong, M.Z., Zhang, M.Q., Wang, H.B., and Zeng, H.M. (2002). Surface modification of magnetic metal nanoparticles through irradiation graft polymerization. Applied Surface Science *200*, 76-93.
4. Rong, M.Z., Zhang, M.Q., Wang, H.B., and Zeng, H.M. (2003). Surface modification of magnetic metal nanoparticles and its influence on the performance of polymer composites. Journal of Polymer Science Part B: Polymer Physics *41*, 1070-1084.
5. Bentley, A.K., Farhoud, M., Ellis, A.B., Nickel, A.-M.L., Lisensky, G.C., and Crone, W.C. (2005). Template Synthesis and Magnetic Manipulation of Nickel Nanowires. J Chem Educ *82*, 765.
6. Gupta, M.K., Kulkarni, D.D., Geryak, R., Naik, S., and Tsukruk, V.V. A Robust and Facile Approach To Assembling Mobile and Highly-Open Unfrustrated Triangular Lattices from Ferromagnetic Nanorods. Nano Lett *13*, 36-42.
7. Krishnadas, K.R., Sajanlal, P.R., and Pradeep, T. Pristine and Hybrid Nickel Nanowires: Template-, Magnetic Field-, and Surfactant-Free Wet Chemical Synthesis and Raman Studies. The Journal of Physical Chemistry C *115*, 4483-4490.
8. Dagani, R. (2002). Tempest in a tiny tube. Chemical & Engineering News *80*, 25-28.
9. Agnew, N.H. (1976). Transition metal complexes of poly(vinylpyridines). Journal of Polymer Science: Polymer Chemistry Edition *14*, 2819-2830.
10. Tsyalkovsky, V., Burtovyy, R., Klep, V., Lupitskyy, R., Motornov, M., Minko, S., and Luzinov, I. Fluorescent Nanoparticles Stabilized by Poly(ethylene glycol) Containing Shell for pH-Triggered Tunable Aggregation in Aqueous Environment. Langmuir *26*, 10684-10692.
11. Zdyrko, B., and Luzinov, I. Polymer Brushes by the "Grafting to" Method. Macromolecular Rapid Communications *32*, 859-869.

12. Toster, J., Iyer, K.S., Burtovyy, R., Burgess, S.S.O., Luzinov, I.A., and Raston, C.L. (2009). Regiospecific Assembly of Gold Nanoparticles around the Pores of Diatoms: Toward Three-Dimensional Nanoarrays. Journal of the American Chemical Society *131*, 8356-8357.
13. Wu, J., Lin, H., Li, J.B., Zhan, X.B., and Li, J.F. (2009). Fabrication and characterization of electrospun mullite nanofibers. Mater Lett *63*, 2309-2312.
14. Wu, J., Lin, H., Li, J.B., Zhan, X.B., and Li, J.F. (2010). Synthesis and Characterization of Electrospun Mullite Nanofibers. Adv Eng Mater *12*, 71-74.
15. Chatterjee, M., Naskar, M.K., Chakrabarty, P.K., and Ganguli, D. (2002). Mullite fibre mats by a sol-gel spinning technique. J Sol-Gel Sci Techn *25*, 169-174.
16. Li, C.S., Zhang, Y.J., and Zhang, J.D. (2009). Polycrystalline Mullite Fibers Prepared by Sol-Gel Method. J Inorg Mater *24*, 848-852.
17. Schmucker, M., Flucht, F., and Schneider, H. (1996). High temperature behaviour of polycrystalline aluminosilicate fibres with mullite bulk composition .1. Microstructure and strength properties. J Eur Ceram Soc *16*, 281-285.
18. Wilson, D.M. (1997). Statistical tensile strength of Nextel(TM) 610 and Nextel(TM) 720 fibres. J Mater Sci *32*, 2535-2542.
19. Naraghi, M., Chasiotis, I., Kahn, H., Wen, Y., and Dzenis, Y. (2007). Novel method for mechanical characterization of polymeric nanofibers. Rev Sci Instrum *78*.
20. Naraghi, M., Chasiotis, I., Kahn, H., Wen, Y.K., and Dzenis, Y. (2007). Mechanical deformation and failure of electrospun polyacrylonitrile nanofibers as a function of strain rate. Applied Physics Letters *91*.
21. Zussman, E., Burman, M., Yarin, A.L., Khalfin, R., and Cohen, Y. (2006). Tensile deformation of electrospun nylon-6,6 nanofibers. Journal of Polymer Science Part B-Polymer Physics *44*, 1482-1489.
22. Tsai, C.C., Mikes, P., Andrukh, T., White, E., Monaenkova, D., Burtovyy, O., Burtovyy, R., Rubin, B., Lukas, D., Luzinov, I., et al. (2011). Nanoporous artificial proboscis for probing minute amount of liquids. Nanoscale *3*, 4685-4695.
23. Gu, Y., and Kornev, K.G. (2013). Alignment of Magnetic Nanorods in Solidifying Films. Particle & Particle Systems Characterization.
24. Hu, H., and Larson, R.G. (2002). Evaporation of a sessile droplet on a substrate. J Phys Chem B *106*, 1334-1344.
25. Tokarev, A., Luzinov, I., Owens, J.R., and Kornev, K.G. (2012). Magnetic Rotational Spectroscopy with Nanorods to Probe Time-Dependent Rheology of Microdroplets. Langmuir *28*, 10064-10071.
26. Kozuka, H. (2006). Stress evolution on gel-to-ceramic thin film conversion. J Sol-Gel Sci Techn *40*, 287-297.
27. Kozuka, H., and Kajimura, M. (2000). Single-step dip coating of crack-free BaTiO3 films > 1 mu m thick: Effect of poly(vinylpyrrolidone) on critical thickness. J Am Ceram Soc *83*, 1056-1062.
28. Gu, Y., Burtovyy, R., Townsend, J., Owens, J.R., Luzinov, I., and Kornev, K.G. (2013). Collective alignment of nanorods in thin Newtonian films. Soft Matter *9*, 8532-8539.

29. Gu, Y., Chen, Z., Borodinov, N., Luzinov, I., Peng, F., and Kornev, K.G. (2014). Kinetics of evaporation and gel formation in thin films of ceramic precursors. Langmuir, DOI: 10.1021/la5037986.
30. Gu, Y., and Kornev, K.G. (2013). Alignment of Magnetic Nanorods in Solidifying Films. Particle & Particle Systems Characterization *30*, 958-963.
31. Andelman, D., and Rosensweig, R.E. (2009). Modulated Phases: Review and Recent Results. Journal of Physical Chemistry B *113*, 3785-3798.
32. Emborsky, C.P., Feng, Z.Z., Cox, K.R., and Chapman, W.G. (2011). Recent advances in classical density functional theory for associating and polyatomic molecules. Fluid Phase Equilibria *306*, 15-30.
33. Eskin, L.D. (1999). On the integral equation describing phase transitions in a system of magnetic rods. Funct. Anal. Appl. *33*, 80-82.
34. Huke, B., and Lucke, M. (2004). Magnetic properties of colloidal suspensions of interacting magnetic particles. Rep. Prog. Phys. *67*, 1731-1768.
35. Osipov, M.A., Teixeira, P.I.C., and daGama, M.M.T. (1997). Density-functional approach to the theory of dipolar fluids. Journal of Physics a-Mathematical and General *30*, 1953-1965.
36. Teixeira, P.I.C., Osipov, M.A., and da Gama, M.M.T. (1998). Phase diagrams of aligned dipolar hard rods. Physical Review E *57*, 1752-1760.
37. Vroege, G.J., and Lekkerkerker, H.N.W. (1992). Phase transitions in lyotropic colloidal and polymer liquid crystals. Rep. Prog. Phys. *55*, 1241-1309.
38. Kornev, K. (1994). Screening Effect and Phase-Transitions in Solutions of Rodlike Dipoles. Physical Review E *49*, 575-582.
39. Tsebers, A.O. (1983). Thermodynamic stability of a suspension of magnetic needles. Magnetohydrodynamics *19*, 146-150.
40. Halsey, T.C. (1992). Elecrorheological fluids. Science *258*, 761-766.
41. Kornev, K.G., Halverson, D., Korneva, G., Gogotsi, Y., and Friedman, G. (2008). Magnetostatic interactions between carbon nanotubes filled with magnetic nanoparticles. Applied Physics Letters *92*, 233117-233113.
42. Gu, Y., Burtovyy, R., Custer, J., Luzinov, I., and Kornev, K.G. (2014). A gradient field defeats the inherent repulsion between magnetic nanorods. Royal Society Open Access *1*, DOI: 10.1098/rsos.140271.
43. Kornev, K.G., Halverson, D., Korneva, G., Gogotsi, Y., and Fridman, G. (2008). Magnetostatic interactions between carbon nanotubes filled with magnetic nanoparticles. Applied Physics Letters *92*, 233117.
44. Wah-Keat, L. (2010). X-ray microtomography of field-induced macro-structures in a ferrofluid. Journal of Magnetism and Magnetic Materials *322*, 2525-2528.
45. Malik, V., Petukhov, A.V., He, L., Yin, Y., and Schmidt, M. (2012). Colloidal Crystallization and Structural Changes in Suspensions of Silica/Magnetite Core–Shell Nanoparticles. Langmuir *28*, 14777-14783.
46. Vorobiev, A., Gordeev, G., Konovalov, O., and Orlova, D. (2009). Surface structure of sterically stabilized ferrofluids in a normal magnetic field: Grazing-incidence x-ray study. Physical Review E *79*, 031403.
47. Lee, W.K. (2010). X-ray microtomography of field-induced macro-structures in a ferrofluid. Journal of Magnetism and Magnetic Materials *322*, 2525-2528.

48. Lee, W.K., and Ilavsky, J. (2013). Particle size distribution in ferrofluid macro-clusters. Journal of Magnetism and Magnetic Materials *330*, 31-36.
49. Wiedenmann, A., Hoell, A., Kammel, M., and Boesecke, P. (2003). Field-induced pseudocrystalline ordering in concentrated ferrofluids. Physical Review E *68*.
50. Heinrich, D., Goni, A.R., Smessaert, A., Klapp, S.H.L., Cerioni, L.M.C., Osan, T.M., Pusiol, D.J., and Thomsen, C. (2011). Dynamics of the Field-Induced Formation of Hexagonal Zipped-Chain Superstructures in Magnetic Colloids. Physical Review Letters *106*.
51. Tokarev, A., Lee, W.K., Sevonkaev, I., Goia, D., and Kornev, K.G. (2014). Sharpening the surface of magnetic paranematic droplets. Soft Matter *10*, 1917-1923.
52. Tokarev, A., Gu, Y., Zakharchenko, A., Trotsenko, O., Luzinov, I., Kornev, K.G., and Minko, S. (2014). Reconfigurable Anisotropic Coatings via Magnetic Field-Directed Assembly and Translocation of Locking Magnetic Chains. Advanced Functional Materials *24*, 4738-4745.
53. Wu, S.-H., and Chen, D.-H. (2003). Synthesis and characterization of nickel nanoparticles by hydrazine reduction in ethylene glycol. Journal of Colloid and Interface Science *259*, 282-286.
54. Zhang, Y., Ding, Y., Gao, J., & Yang, J. (2009). Mullite fibres prepared by sol–gel method using polyvinyl butyral. *Journal of the European Ceramic Society*, *29*(6), 1101-1107.

1.

1. Report Type

Final Report

Primary Contact E-mail

Contact email if there is a problem with the report.

kkornev@clemson.edu

Primary Contact Phone Number

Contact phone number if there is a problem with the report

864-656-6541

Organization / Institution name

Clemson University

Grant/Contract Title

The full title of the funded effort.

Magnetic-field-assisted assembly of ordered multifunctional ceramic nanocomposites for extreme environments

Grant/Contract Number

AFOSR assigned control number. It must begin with "FA9550" or "F49620" or "FA2386".

FA9550-12-1-0459

Principal Investigator Name

The full name of the principal investigator on the grant or contract.

Konstantin G. Kornev

Program Manager

The AFOSR Program Manager currently assigned to the award

Dr. Ali Sayir

Reporting Period Start Date

9/15/2012

Reporting Period End Date

11/14/2015

Abstract

The goal of this project was to explore physics, materials and surface chemistry behind the polymer-based route towards creation of magnetic ceramic composites out of magnetic nanorods and nanofibers. We successfully developed the experimental protocol aimed to make mullite coating films with embedded magnetic inclusions. Electrospun mullite nanofibers with incorporated magnetic nanoparticles, SiC whiskers decorated with magnetic nanoparticles, and Nickel nanorods were successfully embedded into mullite films. We developed an experimental procedure guarantying the reproducible preparation of magnetic silicon carbide (mSiC) whiskers for the use as fillers in the mullite based composite films. We studied kinetics of collective alignment of nanorods and fibers in mullite precursor undergoing a sol/gel transition under uniform magnetic field. These studies resulted in a successful development of the experimental protocol for controlled alignment of nanorods/nanofibers in thin films prior to the complete solidification of the film. We also studied the mechanisms of nanorod-nanorod interactions in non-uniform magnetic fields and developed a robust procedure to control the nanorod placement using a non-uniform field with a designed gradient. Crack-free magnetic composite films with mullite matrix have been synthesized and characterized. Fifteen papers were published based on the results of this project. In 2013, a PhD student, Yu Gu, who worked on this project, was awarded the First Prize in the student paper

competition of the Fiber Society. Mr. Zhaoxi Chen was selected to receive the 2015 Hitachi High Technology Electron Microscope Graduate Fellowship and will continue working on this project studying magnetic phase transformations in nanorods and nanoparticles embedded in mullite film. Two PhD students, Yu Gu and Maryana Nave successfully graduated with the PhD degrees. Thus, the project was scientifically and academically successful.

Distribution Statement

This is block 12 on the SF298 form.

Distribution A - Approved for Public Release

Explanation for Distribution Statement

If this is not approved for public release, please provide a short explanation. E.g., contains proprietary information.

SF298 Form

Please attach your SF298 form. A blank SF298 can be found here. Please do not password protect or secure the PDF The maximum file size for an SF298 is 50MB.

AFD-070820-035.pdf

Upload the Report Document. File must be a PDF. Please do not password protect or secure the PDF . The maximum file size for the Report Document is 50MB.

Final_report_AFOSR_Kornev_Luzinov_Peng.pdf

Upload a Report Document, if any. The maximum file size for the Report Document is 50MB.

Archival Publications (published) during reporting period:

1. Yu Gu and Konstantin G. Kornev, Alignment of magnetic nanorods in solidifying films, Particle & Particle Systems Characterization, DOI: 10.1002/ppsc.201300224 (2013)
2. Yu Gu, Ruslan Burtovyy, James Townsend, Jeffery R. Owens, Igor Luzinov, Konstantin G. Kornev, Collective alignment of nanorods in thin Newtonian films, Soft Matter, Soft Matter, 9, 8532-8539 (2013) (Editor's choice of "HOT PAPER" OF AUGUST 2013)
3. Chen, Z., and Peng, F., "Normal and abnormal grain growths in BaTiO3 fibers." Journal of the American Ceramic Society, 97 [9], 2755-2761 (2014).
4. Townsend, J, Burtovyy, R., Galabura Y., Luzinov I., Flexible chains of ferromagnetic nanoparticles ACS Nano 2014, 8 (7), 6970-6978
5. Yu Gu, Zhaoxi Cheng, Nicolay Borodinov, Igor Luzinov, Fei Peng, and Konstantin G. Kornev, Kinetics of evaporation and gel formation in thin films of ceramic precursors, Langmuir, 30 (48), 14638–14647 (2014)
6. Yu Gu, Ruslan Burtovyy, John Custer, Igor Luzinov, Konstantin G. Kornev "A gradient field defeats the inherent repulsion between magnetic nanorods", Royal Society Open Science, 2014, DOI: 10.1098/rsos.140271
7. Alexander Tokarev , Yu Gu , Andrey Zakharchenko , Oleksandr Trotsenko , Igor Luzinov , Konstantin G. Kornev , and Sergiy Minko, Reconfigurable Anisotropic Coatings via Magnetic Field-Directed Assembly and Translocation of Locking Magnetic Chains, Adv. Funct. Mater. , 24(30), 4738-4745(2014),
8. Yu Gu and Konstantin G.Kornev, Attachment/detachment hysteresis of the fiber-based magnetic grabbers, Soft Matter, 10, 2816-2824 (2014)
9. Alexander Tokarev, Wah-Keat Lee, Igor Sevonkaev, Dan Goia, and Konstantin G.Kornev,
10. Zhaoxi Chen, Yu Gu, Zhao Zhang, Konstantin G. Kornev, Igor Luzinov, and Fei Peng, Measuring flexural rigidity of mullite microfibers using magnetic droplets, Journal of applied physics 117, 214304 (2015).
11. Pavel Aprelev, Yu Gu, Ruslan Burtovyy, Igor Luzinov , and Konstantin G. Kornev, Synthesis and characterization of nanorods for magnetic rotational spectroscopy, Journal of applied physics 118, 074901(2015).
12. Zhaoxi Chen, Zhao Zhang, Chen-Chih Tsai, Konstantin G.Kornev, Igor Luzinov, Minghao Fang, Fei Peng, Electrospun mullite fibers from sol-gel precursor, Journal of sol-gel science and technology, 74, 208-219(2015)
13. Vladislav Vekselman, Luke Sande, and Konstantin G. Kornev, Fully magnetic printing by generation of magnetic droplets on demand with a coilgun, Journal of Aapplied Physics 118, 224902 (2015).

14. Chen Z, Gu, Y., Kornev, K., Luzinov, I., Chen, J., and Peng, F., "Mullite-nickel magnetic nanocomposite fibers obtained from electrospinning and thermal reduction", Journal of American Ceramic Society, DOI: 10.1111/jace.14148 (2016)
15. Gu Y. and Kornev K.G. Ferromagnetic Nanorods in Applications to Control of the In-Plane Anisotropy of Composite Films and for In Situ Characterization of the Film Rheology, Advanced Functional; Materials, DOI: 10.1002/adfm.201504205 (2016). (Invited Feature Article)

Changes in research objectives (if any):

Change in AFOSR Program Manager, if any:

Extensions granted or milestones slipped, if any:

AFOSR LRIR Number

LRIR Title

Reporting Period

Laboratory Task Manager

Program Officer

Research Objectives

Technical Summary

Funding Summary by Cost Category (by FY, $K)

	Starting FY	FY+1	FY+2
Salary			
Equipment/Facilities			
Supplies			
Total			

Report Document

Report Document - Text Analysis

Report Document - Text Analysis

Appendix Documents

2. Thank You

E-mail user

Mar 25, 2016 21:33:02 Success: Email Sent to: kkornev@clemson.edu